Beyond Steady-State Lamellar Eutectic Growth

Alain Karma
California Institute of Technology, Pasadena, California 91125
(Received 16 March 1987)

Lamellar eutectics only grow in steady state over a small range of melt compositions between the two solidus lines of a binary phase diagram. Outside this range their growth exhibits a rich dynamical behavior. A random-walk model is constructed to simulate eutectic solidification of a thin film and applied to study this behavior. In addition to oscillatory modes, a "tilting instability" on the lamellar spacing is found at off-eutectic compositions. Well into nonlinear regimes, this instability causes lamellae from the minor phase to follow convoluted solidification paths thereby generating exotic eutectic textures.

PACS numbers: 61.50.Cj, 05.70.Ln, 64.70.Dv, 81.30.Fb

The theoretical model of Jackson and Hunt[1] permits steady-state lamellar eutectic growth to take place at all melt compositions between the two solidus lines of a binary eutectic phase diagram. However, in practice, steady-state growth is limited to a small range of melt compositions in the vicinity of the eutectic composition. Our experimental and theoretical knowledge of the wide variety of non-steady-state modes of growth which can occur outside this range has remained very limited. On the experimental side, the best documented non-steady-state behavior is one in which dendrites of one solid phase and lamellar eutectics both coexist.[2] This situation is observed at off-eutectic compositions when the growth of one solid phase becomes sufficiently enhanced to cause dendrites of this phase to emerge ahead of the eutectic interface. There is also experimental evidence for dynamical modes of growth in which dendrites are absent.[3] One of them is an oscillatory mode on twice the lamellar spacing which causes lamellae from the minor phase (the phase of smaller volume fraction) to follow sinusoidal solidification paths, as opposed to the vertical paths followed during steady-state growth. Other modes, which seem to involve more convoluted solidification paths of these lamellae, generate complex eutectic patterns ranging from orderly to chaotic.

One important tool which is missing at this point to develop a systematic understanding of the mechanisms underlying the formation of these intricate eutectic solidification patterns is a numerical algorithm capable of simulating the motion of a eutectic solidification front. To construct such an algorithm, even for the simplest two-dimensional situation characteristic of thin films, represents a formidable task since one must add the constraint of mechanical equilibrium at solid-solid-liquid triple points (where three phases meet in space) to the already existing difficulties of the free-boundary problem for a single solid phase. The main purposes of this Letter are, first, to show how this task can be accomplished by the extension to three phases of the random-walk model developed by Kadanoff,[4] Tang,[5] and Liang[6] for viscous flow in a Hele-Shaw cell, and, second, to show that these patterns which have been observed experimentally can be understood as consequences of diffusional instabilities occurring on the scale of the lamellar spacing at sufficiently off-eutectic melt compositions. In addition, our results demonstrate the practical utility of random-walk computational methods for simulating realistic models of complex processes.

We consider the simplest situation of free eutectic growth at fixed thermal undercooling $\Delta T = T_E - T_0$ in the absence of temperature gradient, where T_E and T_0 are respectively the eutectic temperature and the isothermal temperature of the interface. The Jackson-Hunt model for free growth predicts a one-parameter family of steady states with lamellar spacings and growth velocities related by

$$v = v_m \left(2/\Lambda - 1/\Lambda^2\right), \quad \Lambda = \lambda/\lambda_m, \tag{1}$$

where $\lambda_m \sim (\Delta T)^{-1}$ is the spacing at which the growth velocity reaches its maximum value $v_m \sim (\Delta T)^2$. We further restrict our attention to the experimentally relevant limit of small thermal undercoolings where growth occurs slowly and the diffusion equation can be approximated by the Laplacian. The motion of the eutectic interface is then governed by

$$\nabla^2 u = 0, \tag{2}$$

conservation of mass at both solid-liquid interfaces,

$$V_n = -\hat{\mathbf{n}} \cdot \nabla u, \quad \alpha \text{ phase}, \tag{3a}$$

$$QV_n = \hat{\mathbf{n}} \cdot \nabla u, \quad \beta \text{ phase}, \tag{3b}$$

local thermodynamic equilibrium at the interface (Gibbs- Thomson relations),

$$u(\alpha) = \Delta T m_\alpha^{-1} - d_\alpha \kappa, \quad \alpha \text{ phase}, \tag{4a}$$

$$u(\beta) = -\Delta T m_\beta^{-1} + d_\beta \kappa, \quad \beta \text{ phase}, \tag{4b}$$

and the constraint of mechanical equilibrium which requires the sum of surface tensions to vanish at a triple

point,

$$\sigma_{L\alpha}\hat{\mathbf{t}}_{L\alpha}+\sigma_{L\beta}\hat{\mathbf{t}}_{L\beta}+\sigma_{\alpha\beta}\hat{\mathbf{t}}_{\alpha\beta}=\mathbf{0}, \quad (5)$$

where $\hat{\mathbf{t}}_{\gamma\nu}$ is a unit vector which is tangent to the γ-ν interface at a triple point and points away from this point. Here $\sigma_{\alpha\beta}$ is the α-β surface tension, σ_{LS} is the L-S surface tension, m_s is the liquidus slope of each phase dT/du defined to be positive, $d_s=\sigma_{Ls}T_E/m_sL_s$ and L_s are respectively the capillary length and latent heat per unit volume of each phase ($s=\alpha,\beta$), κ is the local interfacial curvature, $u\equiv(C-C_E)/\Delta C$ is a dimensionless composition field where C denotes the concentration of one of the components, for example, the number of B molecules per unit volume for a two-component system consisting of A and B molecules, C_s is the concentration of each solid phase, $\Delta C\equiv C_\beta-C_\alpha>0$ is the miscibility gap, C_E is the eutectic concentration, and C_∞ is the concentration in the sample far ahead of the solidification front. In addition, we have defined $V_n=(-u_\alpha)v_n/D$ where v_n is the local normal velocity of the interface, D is the coefficient of solute diffusivity, and $Q\equiv u_\beta/(-u_\alpha)$ with $u_s\equiv(C_s-C_E)/\Delta C$ ($u_\alpha<0$, $u_\beta>0$). Finally, the exponentially decaying part of u in the upward z direction is translated, in the Laplacian limit of the diffusion equation, into a linear gradient boundary condition on u far ahead of the interface where, in steady state,

$$(\partial_z u)_\infty=(v/D)(C_\infty-C_E)/\Delta C\equiv(v/D)u_\infty,$$

with $C_\infty=C_\alpha\eta+C_\beta(1-\eta)$; $\eta\equiv\lambda_\alpha/\lambda$ is the volume fraction of the α phase, λ_s ($s=\alpha,\beta$) is the lamellar width of each phase, and $\lambda=\lambda_\alpha+\lambda_\beta$ is the lamellar spacing.

We now describe a random-walk model which can simulate Eqs. (2)–(5). The model and its results are only briefly described here and a more detailed exposition will be given elsewhere.[7] Points on a two-dimensional square lattice are divided into three categories: α and β sites (s sites; $s=\alpha,\beta$) represent sites occupied by the solid α and solid β phases, respectively, and empty sites (e sites), those occupied by the liquid phase. The lattice spacing is set equal to unity and W measures the lateral width of the system where periodic boundary conditions are imposed at the end points. The interface, from which walkers are released, is composed of all s sites which have at least one bond connected to an e site (i.e., the solid-liquid interface). The composition field u is interpreted as the probability density of random walkers which is well known to satisfy the Laplace equation. Accordingly, the probability of a walker being released from a particular s site is given by $u(s)$, the value of u on the interface. Since $u(s)$ can be both positive and negative we use the normalized probability distribution $P(s)\equiv|u(s)|/\max\{|u|\}$ and assign to walkers a flux $f(s)$ equal to the sign of $u(s)$ [$f(s)=\pm1$], where $\max\{|u|\}$ is the maximum value of $|u|$ on the interface. Each s site on the interface is then checked sequentially and a random walker carrying a flux $f(s)$ is released with probability $P(s)$. The walk is terminated when the walker returns to any s site. The net flux of walkers in all s—e bonds joining s and e sites is recorded. For each walk the flux $f(s,e)$ in the s—e bond through which the walker leaves the interface is increased by $f(s)$ and the flux in the s'—e' bond through which it returns is decreased by $f(s)$. Interface motion at site s is controlled by the normal gradient of u at the interface, $u(s)-u(e)$, which is proportional to the flux in the corresponding s—e bond $\{f(s,e)\sim[u(s)-u(e)]/4\}$. Accordingly, the sum $\sum_s f(s,e)$ of fluxes in all s—e bonds connected to a given e site is evaluated. This site then becomes occupied by an α site if at least one of the s—e bonds is of type α—e and the sum $\sum_s f(s,e)$ exceeds an integer M, or by a β site if at least one of the bonds is of type β—e and $\sum_s f(s,e)$ is less than $-QM$ [see Eqs. (3)]. Similarly, an s site is emptied (melting) when the sum $\sum_e f(s,e)$ of fluxes in all bonds connected to this site is less than $-M$ for $s=\alpha$ or exceeds QM for $s=\beta$. When M is large many walks take place during the time necessary for the interface to move one lattice unit and fluctuations in the normal gradient of u at the interface are therefore diminished. In the limit $M\to\infty$ deterministic equations of motion are simulated. Finally, walkers are released from infinity at off-eutectic compositions to simulate the gradient boundary conditions on u.

The last task is to build into the model the constraint of mechanical equilibrium [Eq. (5)]. To do so we derive a form of the Gibbs-Thomson relation which takes into account the interaction energy between the three phases at triple points. Away from these points this form reduces to Eqs. (4). In their vicinity, that is, within a distance r of triple points where r measures the range of the interaction energy between different phases, this form causes the composition field $u(s)$ to beome large when slight deviations from the constraint of mechanical equilibrium occur. This increase in composition in turn induces large normal composition gradients which cause interface motion to smooth out these deviations in a time much shorter than the time it takes for triple points to move a distance r. Consider the thermodynamic potential corresponding to the interfacial region $\Omega_r=\sum_s\Omega_r(s)$, where

$$\Omega_r(s)=-\mu_\alpha N_\alpha-\mu_\beta N_\beta-\mu_L N_L+a_{\alpha\beta}N_\alpha N_\beta+a_{\alpha L}N_\alpha N_L+a_{\beta L}N_\beta N_L, \quad (6)$$

μ_ν is the chemical potential of each phase ($\nu=\alpha,\beta,L$), N_ν is the number of lattice sites of each phase contained inside a circle of radius r centered on site s, and $a_{\gamma\nu}$ measures the strength of the interaction energy between the γ and ν phases. The corresponding Gibbs-Thomson relation is then obtained by our imposing the requirement that Ω_r be stationary against infinitesimal interface deformations equivalent to addition or withdrawal of a surface site: $\partial\Omega_r(s)/\partial N_\alpha=\partial\Omega_r(s)/\partial N_\beta=0$, with the con-

straint $N_\alpha+N_\beta+N_L=N_r$, where N_r is the total number of sites inside the circle of radius r ($N_r=\pi r^2$ for $r\gg 1$), and further by our using the fact that $u(\alpha)-m_\alpha^{-1}\Delta T \propto \mu_L-\mu_\alpha$ and $u(\beta)+m_\beta^{-1}\Delta T\propto\mu_\beta-\mu_L$. We obtain

$$u(\alpha)-m_\alpha^{-1}\Delta T=-a_{\alpha L}(N_L-N_\alpha)+(a_{\beta L}-a_{\alpha\beta})N_\beta, \tag{7a}$$

$$u(\beta)+m_\beta^{-1}\Delta T=a_{\beta L}(N_L-N_\beta)-(a_{\alpha L}-a_{\alpha\beta})N_\alpha, \tag{7b}$$

where the constants of proportionality between $\mu_L-\mu_s$ and $u(s)\pm m_s^{-1}\Delta T$ have been absorbed by a suitable redefinition the $a_{\gamma\nu}$'s, and Eqs. (7) determine $P(s)$.[8] Away from triple points the second terms on the right-hand sides of Eqs. (7) vanish and N_L-N_s is proportional to the interfacial curvature: $\kappa=B(r)(N_L-N_s)/r^3$, where $B(r)\to\frac{3}{2}$ for $1\ll r\ll\kappa^{-1}$. Equations (7) therefore reduce to the form of Eqs. (4). Finally, for $u(s)$ to be continuous at a triple point the right-hand sides of Eqs. (7) have to scale as r/λ and vanish in the limit $r/\lambda\to 0$. This requirement and the constraint $N_\alpha+N_\beta+N_L=N_r$ then fix uniquely N_α, N_β, and N_L within a circle of radius r centered at this point, and consequently the directions of the $\hat{\mathbf{t}}_{\gamma\nu}$'s, in terms of the $a_{\gamma\nu}$'s (which also relates the $a_{\gamma\nu}$'s with the $\sigma_{\gamma\nu}$'s).

We restrict our attention to a symmetrical binary eutectic phase diagram with $m_\alpha=m_\beta\equiv m$ and $Q=1$, which implies $\eta=\frac{1}{2}-u_\infty$, and choose equal surface tensions $a_{\alpha L}=a_{\beta L}=a_{\alpha\beta}\equiv aB(r)/r^3$, which implies $N_\alpha=N_\beta=N_L=N_r/3$ and equal 120° angles between the $\hat{\mathbf{t}}_{\gamma\nu}$'s at a triple point as shown in Fig. 1 (here these angles differ slightly from 120° because of the inherent anisotropy of the lattice). All our simulation results are parametrized in terms of u_∞ and Λ [Eq. (1)]. Measured values of v vs Λ agree with Eq. (1) within 20% and, for $\Lambda<1$ simulations with about ten lamellae ($W=5\lambda$), exhibit the classic long-wavelength instability leading to termination of lamellae.[7] At sufficiently off-eutectic compositions we observe two short-wavelength instabilities [Figs. 2(a) and 2(b)]: the oscillatory instability at twice λ predicted successfully by the discrete stability analysis of Dayte and Langer,[9] and a new tilting instability on the lamellar spacing which forces lamellae from the phase of smaller volume fraction (β phase here) to bend coherently on one side of the vertical growth axis. The latter was missing in the stability analysis of Dayte and Langer since the discrete model on which their calculation is based cannot describe triple-point displacements caused by interfacial deformations within individual lamellae. At fixed Λ the tilting instability first occurs at a more off-eutectic composition (larger value of $|u_\infty|$) than the oscillatory one, and at fixed composition it occurs at a larger value of Λ. In simulations with $u_\infty=-\frac{1}{6}$ and $W=2\lambda$, oscillations terminate steady-state lamellar growth when $\Lambda>\Lambda_{os}\simeq 1$, while in simulations with the same value of u_∞ and $W=\lambda$, steady states become unstable against tilting when $\Lambda>\Lambda_{ti}\simeq 1.5$.

The appearance of both oscillatory and bending modes can be explained physically by consideration of the destabilizing effect of the composition gradient ahead of the interface, $(\partial_z u)_\infty=vu_\infty/D$, present at off-eutectic compositions. The idea that instability of a lamellar eutectic front can arise as a consequence of this effect was

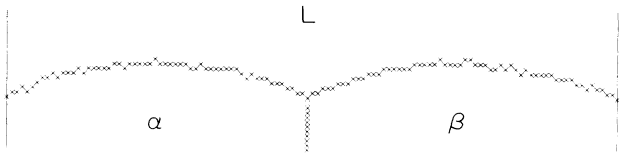

FIG. 1. Steady-state interface at exactly eutectic composition in a situation where equal surface tensions balance at a solid-solid-liquid triple point. The width of the system W is 121 lattice units. Sites on the boundary between any two phases are represented by crosses.

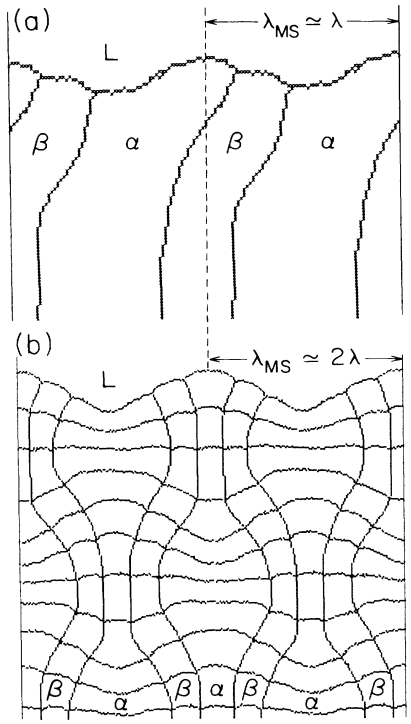

FIG. 2. Interface deformations associated with (a) tilting instability and (b) oscillatory instability. The lamellae bend in response to a bulge in the interface to preserve the balance of surface tensions at triple points. (a) $W=\lambda=61$ and $\Lambda=1.8$, (b) $W=2\lambda=121$ and $\Lambda=1.1$, and in both (a) and (b) $M=15$, $r=5$, and $u_\infty=-\frac{1}{6}$. (b) shows only the late stages of a simulation that started from a slightly perturbed steady-state growth.

pointed out previously by Hurle and Jakeman.[10] First, note that in the presence of such a gradient an initially planar single solid phase (α phase here if we treat the lamellar eutectic as a single phase) will develop during its growth a spatially sinusoidal deformation of wavelength $\lambda_{MS} \sim (d_\alpha / |(\partial_z u)_\infty|)^{1/2}$ as a result of the classic Mullins-Sekerka instability.[11] Then equating the spatial period of the interface deformation corresponding to each mode with λ_{MS} [as shown in Figs. 2(a) and 2(b)] yields the criterion that oscillations and tilting should first occur when $\lambda_{MS}=2\lambda$ and $\lambda_{MS}=\lambda$, respectively. These two equalities in turn define two lines in the (u_∞, Λ) plane, each line representing the neutral stability boundary of each mode.[7]

What happens above the onset of short-wavelength instabilities? We find that although these instabilities terminate steady-state growth they do not necessarily lead directly to the appearance of dendrites. A rich dynamical behavior can take place in between steady states and dendrites within some range of spacings and compositions. The general understanding of this behavior emerging so far from our simulations is that when either instability (oscillatory or tilting) dominates the dynamics, coherent structures are formed, while in regions where both instabilities compete the motion of lamellae can become chaotic. The most stunning observation is that the coherent structures formed when tilting dominates are composed of convoluted solidification paths of β lamellae as shown in Fig. 3(a). The dynamical mechanism responsible for one convolution is explained in a time sequence shown in Figs. 3(b) and 3(c). This sequence provides a good example of catastrophic dynamical events which can be successfully described by our algorithm. Solid β lamellae bend sufficiently for their tips to come in contact with the solid α phase. Figure 3(b) is a snapshot taken just before contact. After contact, two new triple points are created and the solidification path splits two ways. One path solidifies upwards and the other downwards inside a liquid pocket which becomes ultimately filled with solid β. Figure 3(c) is a snapshot taken when the liquid pocket is almost completely solidified.

Finally, it is worth noting that Fig. 3(b) bears a striking resemblance to an experimental photograph displayed in the classic paper by Jackson and Hunt (Fig. 15 in Ref. 1) and that there also seems to be evidence for eutectic structures similar to the one displayed in Fig. 3(a).[3] Additional systematic experimental studies of off-eutectic solidification of thin films are strongly needed at this point: first, to explore further the range of possible microstructures, and, more fundamentally, to investigate complex spatiotemporal behaviors ranging from orderly to chaotic.

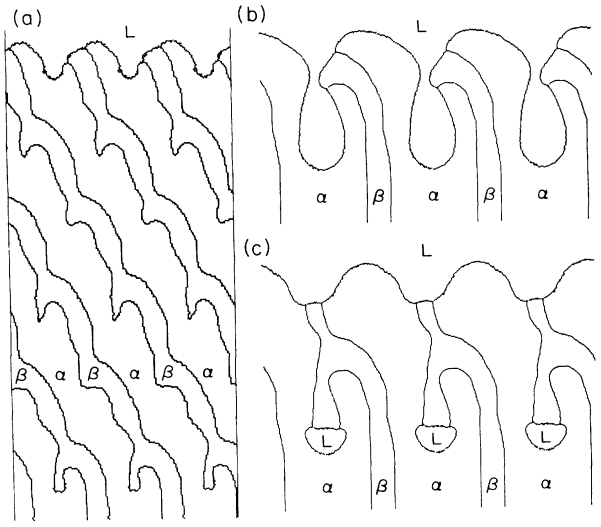

FIG. 3. (a) Exotic eutectic texture; $u_\infty = -\frac{1}{6}$, $W=\lambda=61$, $M=15$, $r=5$, and $\Lambda=3$. This run took about 30 h of central-processing-unit time on a Ridge computer. (b),(c) $W=\lambda=121$, $\Lambda=2$, $u_\infty=-\frac{1}{4}$, $M=10$, and $r=5$.

The author thanks M. C. Cross for many helpful discussions. This research is supported by the California Institute of Technology through a Weingart Fellowship and through the Program in Advanced Technologies which is funded by General Motors, GTE, TRW, and Aerojet.

[1]K. A. Jackson and J. D. Hunt, Trans. Metall. Soc. AIME **236**, 1129 (1966).

[2]D. P. Woodruff, *The Solid-Liquid Interface* (Cambridge Univ. Press, Cambridge, 1973).

[3]J. Van Suchtelin, unpublished.

[4]L. P. Kadanoff, J. Stat. Phys. **39**, 267 (1985).

[5]C. Tang, Phys. Rev. A **31**, 1977 (1985).

[6]S. Liang, Phys. Rev. A **33**, 2663 (1986).

[7]A. Karma, to be published.

[8]Because of limited computation time, simulations are performed with values of r and λ ($r \simeq 5$, $\lambda \simeq 60$) which introduce corrections to the continuum limit of order $1/r$ and r/λ and require the use of slightly modified versions of Eqs. (7) near triple points to ensure that deviations from mechanical equilibrium at these points relax much faster than λv^{-1}.

[9]V. Dayte and J. S. Langer, Phys. Rev. B **24**, 4155 (1981).

[10]D. T. J. Hurle and E. Jakeman, J. Cryst. Growth **3,4**, 574 (1968).

[11]W. W. Mullins and R. F. Sekerka, J. Appl. Phys. **35**, 444 (1964).